Experiments with reduced single pass absorption at ASDEX Upgrade – instrumentation and applications

Martin Schubert[1*], *Joerg* Stober[1], *Albrecht* Herrmann[1], *Eduard* Grigore[2], *Walter* Kasparek[3], *Carsten* Lechte[3], *Francesco* Monaco[1], *Bernhard* Petzold[1], *Burkhard* Plaum[3], *Emanuele* Poli[1], *Cristian* Ruset[2], *Stefan* Vorbrugg[1], *Dietmar* Wagner[1], and ASDEX Upgrade Team[4]

[1]Max-Planck-Institut f. Plasmaphysik, Boltzmannstr. 2, D-85748 Garching b. München, Germany
[2]Institute for Laser, Plasma and Radiation Physics, Atomistilor Street 409, RO-077125 Magurele-Bucharest, Romania
[3]Institut f. Grenzflächenverfahrenstechnik und Plasmatechnologie, Pfaffenwaldring 31, D-70569 Stuttgart, Germany
[4]see author list of *Ulrich* Stroth, *et al.*, Nucl. Fusion **62**, 042006 (2022)

Abstract. Reflecting gratings have been installed in the vacuum vessel of ASDEX Upgrade for all beamlines of the electron cyclotron resonance heating system. Potentially unabsorbed millimetre wave power after the first pass through the plasma is redirected towards the plasma centre. This increases the efficiency of heating schemes with reduced single pass absorption like O-2 or X-3. In order to monitor beam position and power, thermocouples were installed into the gratings. A numerical model was developed to evaluate the beam intensity during short pulses from the thermocouple measurement in a non-stationary environment. An experiment was carried out, where only the X-3 resonance is present in the plasma, and the millimetre wave beam shine-through was measured successfully as a function of the central plasma electron temperature. This allows to deduce the X-3 absorption experimentally. Scanning the launching angles, it seems possible to measure the 2D beam cross section after the first pass through the plasma.

1 Introduction

The electron cyclotron resonance heating system (ECRH) at ASDEX Upgrade (AUG) has been extended to eight Gyrotrons in total. Each Gyrotron operates at 105 and 140 GHz and is designed for up to 1 MW millimetre wave output power. Experimental topics at AUG include variations of the main magnetic field strength in the plasma and conditions with high plasma densities, potentially above the X-2 cut-off at 140 GHz, e.g. [1]. New ECRH schemes have been proposed [2] which can cope with the demand, at the cost of reduced single pass absorption, however. It is necessary to design reflecting gratings [3] and install them into the heat shield, i.e. the inner column inside AUG's vacuum vessel. The gratings are designed for 140 GHz, they are refocussing and redirecting each beam towards the plasma centre, thereby increasing the second-pass absorption and the total heating efficiency.

Part of the heat shield inside AUG consists of the steel W1.4901. Four of the gratings were manufactured out of this steel and a thin tungsten coating was applied, which is a newly developed technique. In order to monitor the position of each ECRH beam on the corresponding grating, thermocouples were installed. The fast response of the thermocouples opens the possibility to measure the local beam intensity after the first pass through the plasma with short pulses. Since experimental data on X-3 absorption at 140 GHz are rare, it was decided to try this measurement. The experimental setup uses the two available frequencies: (a) 105 GHz at different power levels and with nearly perfect absorption at the X-2 resonance in order to vary the central plasma electron temperature. (b) 140 GHz for the probing beam, where only the X-3 resonance is present in the plasma and the shine-through can be measured at the heat shield, using the thermocouples. The results on X-3 absorption are presented in a separate contribution to this conference.

In a more general approach to study the beam properties after the first pass through the plasma, we started to measure the local beam intensity as a function of the launching direction, in a set of reproducible and similar plasma discharges using the O-2 mode polarisation. Putting the measurements of several AUG experiments together, a kind of 2D image of the beam cross-section can be generated.

2 Two-pass scheme at ASDEX Upgrade

The design criteria were already written down [3] and the scheme has now been completed for all ECRH launchers (figure 1). We would like to point out that the oblique geometry is necessary in order to maximize the O-2 absorption [2]. For each launcher (figure 2) there is a corresponding reflecting grating (figure 3) and it is necessary that the unabsorbed beam power after the first pass is located on the corresponding grating, as long as the absorption is incomplete. Consequently, the heating

* Corresponding author: Martin.Schubert@ipp.mpg.de

geometry is fixed and no large variations of the launching direction are allowed.

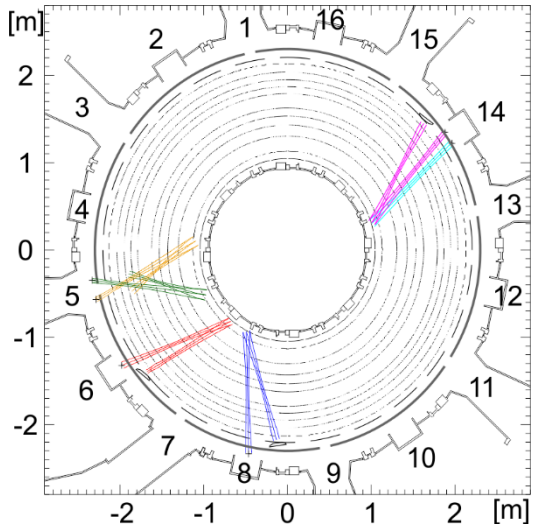

Fig. 1. Schematic top view on the plasma midplane cross section of ASDEX Upgrade, two-pass ECRH heating beams are shown in colour. The vacuum vessel consists of 16 segments. ECRH launchers are located in segments 5,6,8 and 14. Since the four launchers in segment 5 would shadow each other in this view, only two of them are shown for simplicity. The beam trajectories in segment 5 do not start or end in the midplane, they have a significant vertical component and appear shortened in the projection of this view.

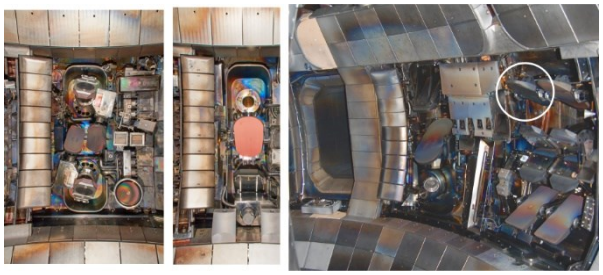

Fig. 2. ECRH launchers inside the AUG vacuum vessel, the view is radially outward. Left: Double launcher in segment 14. Middle: Single launcher in segment 8. Right: Segments 7,6,5 (from left to right) with the large port of the neutral beam input in segment 7, the single ECRH launcher in segment 6, and the four launchers in segment 5. The robust surfaces of the auxiliary limiters left of the launcher mirrors in segments 14, 8, and 6 are the design end points after the second pass. The launcher highlighted with a white circle in segment 5 (right photo) was used for the experiments described in section 4.

The inner column of AUG's vacuum vessel consists of tiles (figure 3). Two tiles at the corresponding position were merged into a double tile, to make the reflecting gratings sufficiently large. The heat shield around the midplane consists of W1.4901 steel, which concerns the gratings in segments 7 and 13 (figure 3). The other ones were machined out of graphite.

With tungsten coating, mm-wave power absorption of the grating can be reduced to approx. 0.5% [4]. For graphite, this coating is established at AUG for a long time, while for W1.4901 steel this had to be developed. Figure 4 shows the depth profile measured by glow discharge optical emission spectroscopy (GDOES) of a successful coating. A thin coating of up to 10 µm can be applied to this steel using a molybdenum interlayer.

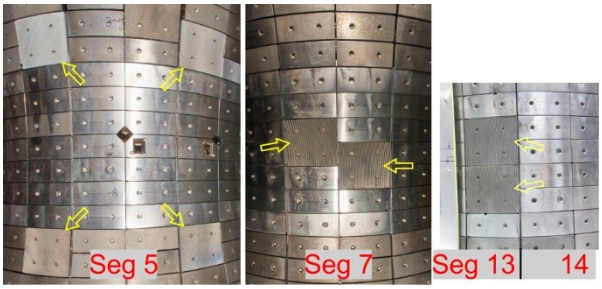

Fig. 3. AUG vacuum vessel heat shield, which consists of tiles. The view is radially inward towards the central column of the machine. The visible double tiles are the reflecting gratings that correspond to the launchers from figure 2. Left: Four gratings for the launchers of segment 5. Note, that the gratings are not in the midplane. Middle: Two gratings in segment 7 for the two single launchers of segments 6 and 8. Right: Two gratings in segments 13 for the double launcher of segment 14.

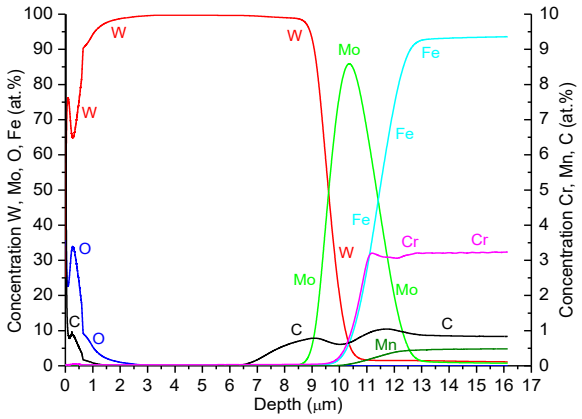

Fig. 4. Depth profiles of W, Mo, Fe, Cr, Mn, C and O measured by Glow Discharge Optical Emission Spectroscopy (GDOES) on W-coated sample made of W1.4901 steel. Near the surface of the sample (0…8 µm), we have almost pure tungsten (W). The molybdenum (Mo) interlayer is found in a depth of approx. 10 µm. For depths > 12 µm we find the expected composition of W1.4901 steel (Fe, Cr, C, Mn etc). GDOES is sputtering the sample and is, thus, destructive.

3 Thermocouple measurement

Fast thermocouples can be used to monitor ECRH beam positions in scenarios with potential shine-through [2], and this technique has been developed continuously [5]. We chose a NiCr-Ni (type K) thermocouple with an outer diameter of 0.25 mm [6]. Sensitivity 40.96 µV/K and maximum specified temperature approx. 1200 ºC. The jacket of the thermocouple is made of Inconel 600 and it is connected to a flexible cable within a cylindrical joint with outer diameter 4 mm and a length of 25 mm. We have tested different mount options and found that the best compromise between longevity and signal amplitude is achieved in a flush mount (figure 5).

3.1 Flush mount

Several tools have been developed in order to facilitate the flush mount, cf. figure 6. We have put emphasis on sufficient protection and shielding of the cables in order to prevent damage during operation with mm-waves.

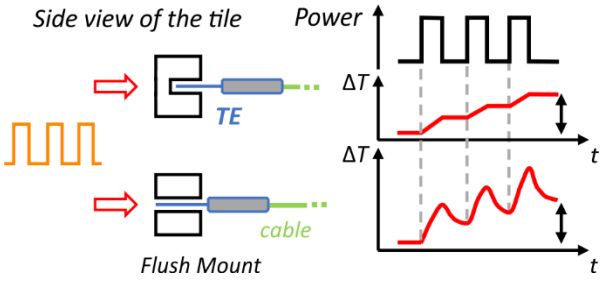

Fig. 5. Schematic comparison of thermocouple (TE) mount options and signal response on an incoming pulse train of mm-wave power. Top: Mounted from the rear inside the bulk material. Bottom: Flush mount, the borehole goes through the surface and the TE is partly exposed to the mm-wave. The On/Off time of the power is of the same order as the relaxation time of the thermocouple. If the total heat capacity of the absorbing material is comparable, then the total temperature rise after the last pulse plus relaxation time is also comparable (double sided arrows on the right).

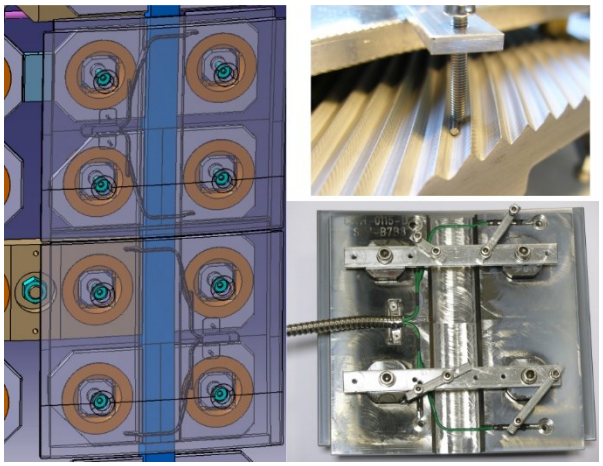

Fig. 6. Left: Transparent CAD view of two double tiles with built-in channels for the cables. Right: Tools which ensure a precise flush mount. During the attachment procedure, the opening of the borehole at the plasma exposed surface is temporarily blocked (upper right photo). This opening is normally located on the bottom of a groove of the grating. The view onto the rear side (lower right) shows the mechanics used to fixate cables and cylindrical joints.

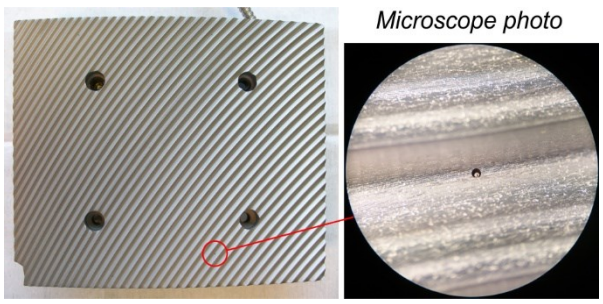

Fig. 7. Complete assembly of a reflecting grating, tungsten coated and equipped with thermocouples. Left photo: plasma facing side, width and height approx. 20 cm and 18 cm. The four large openings are for attaching the tile to the heat shield. Right: magnified area around a 0.5 mm borehole, containing a flush mounted thermocouple with a diameter of 0.25 mm.

In the manufacturing process the thermocouples are attached to the tile with a graphite glue, which is a mixture of graphite powder and phenolic resin. The tile including thermocouples and cables is baked, until the graphite glue is sufficiently stable. After complete assembly, tile and grating are inspected (figure 7). If the flush mount was successful, then within each borehole the tip of the thermocouple is clearly visible.

During the recent AUG experimental campaigns we did not encounter thermocouple sensor failures specific to the flush mount. In the AUG case, the specified temperature ranges of the thermocouple sensor and jacket [6] are not exceeded. This should be regularly checked, depending on the planned application.

3.2 Evaluation model

During experiments with applied mm-wave power, Gyrotron On/Off times are recorded with a precision better than 0.1 milliseconds (ms) by directional couplers in the transmission line. The thermocouple signals are filtered with a 300 Hz Bessel low-pass and recorded with 1 ms time resolution. Taking into account the relevant transit times and the transfer function of the filter, we observe a characteristic time delay of typically 10 ms between the mm-wave power arriving at the borehole and the start of the signal rise in the recorded thermocouple signal. The relaxation time of the signal, when the mm-power is switched off, is of the same order. This indicates that, when evaluating short pulses, the model should be comprehensive enough to account for the effect of these time constants.

Thermocouples, which are not hit by the mm-wave, show a continuous, uniform, and slow rise of the temperature due to the background heat load from the plasma. The rise time is larger than the relaxation time of the thermocouple. We therefore model this background heat load p_{bg} homogeneously across the tile, based on the direct measurement from those thermocouples.

When evaluating pulsed mm-wave power similar to figure 5 (bottom), we use a simplified 2D model around each thermocouple in order to account for the dynamics of the heat exchange between the absorbing surface and the thermocouple sensor, which is located several 10 µm below the surface [6], see also figure 8.

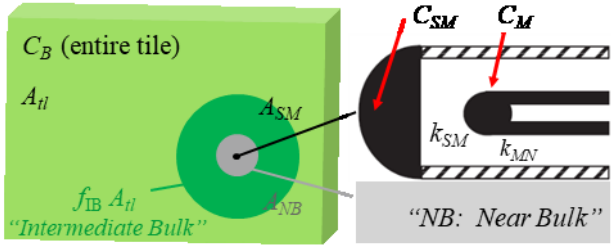

Fig. 8. Schematic visualisation of model temperature zones around and inside a thermocouple. Left: The entire tile with total heat capacity C_B and exposed surface area A_{tl}. Cylindrical zones around the thermocouple, which expand into the depth: near bulk A_{NB} (grey) and intermediate bulk $f_{IB}\,A_{tl}$ (fraction of A_{tl} dark green). Right: side view of the thermocouple cross section [6]. Absorbing surface area A_{SM} with heat capacity C_{SM}. The metal-metal joint with the heat capacity C_M is the position of the temperature measurement T_M and it is located several 10 µm below the surface [6]. The heat flux has to cross insulating material with model heat conductances k_{SM} and k_{MN}.

The model has three grid points in radial direction parallel to the tile surface, and one additional grid point in the depth, where the measurement T_M takes place (figure 8). The three radial grid points are: (i) absorbing tip of the thermocouple with surface area A_{SM}, heat capacity C_{SM}, temperature T_{SM} , (ii) the near bulk with surface area $A_{NB} = f_{NB}\, A_{tl}$, temperature T_{NB}, and (iii) the intermediate bulk with surface area $A_{IB} = f_{IB}\, A_{tl}$, temperature T_{IB}.

Both near and intermediate bulk are characterized as fractions f_{NB} and f_{IB} of the entire tile, i.e. with heat capacities $C_{NB} = f_{NB}\, C_B$, and $C_{IB} = f_{IB}\, C_B$, respectively.

We introduce heat conductances: k_{SM} between the thermocouple tip and the measurement sensor (C_M, T_M), k_{MN} between the sensor and the near bulk, and k_{NB} between near and intermediate bulk. For simplicity, we allow heat transfer from T_{NB} to T_{IB} (via k_{NB}) as a loss term for T_{NB}, but we set T_{IB} as a boundary condition, which changes its value only due to the heat flux from the surface, ignoring the incoming radial transfer from the near bulk. In doing so, we assume that at this position, the incoming heat flow from the near bulk is small compared to the flow from the surface, and we end up with a system of three coupled differential equations for T_{SM}, T_M, T_{NB}, and a separate equation for T_{IB}:

$$C_{SM}\,\dot{T}_{SM} = A_{SM}\,(p_{bg} + p_A) - k_{SM}\,(T_{SM} - T_M) \qquad (1)$$

$$C_M\,\dot{T}_M = k_{SM}\,(T_{SM} - T_M) - k_{MN}\,(T_M - T_{NB}) \qquad (2)$$

$$f_{NB}\,C_B\,\dot{T}_{NB} = f_{NB}\,A_{tl}\,(p_{bg} + p_A) + k_{MN}\,(T_M - T_{NB}) - k_{NB}\,(T_{NB} - T_{IB}) \qquad (3)$$

$$f_{IB}\,C_B\,\dot{T}_{IB} = f_{IB}\,A_{tl}\,(p_{bg} + r_{IB}\cdot p_A) \qquad (4)$$

In this system p_A is the absorbed mm-wave intensity, p_{bg} is the (homogeneous) background intensity, measured by the distant thermocouples, and the term $r_{IB}{\cdot}p_A$ is to model the heat flux to the intermediate bulk as a fraction of the mm-wave intensity. The fraction r_{IB} had to be introduced in order to correct the baseline of the signal, whenever the incoming mm-wave intensity is zero for a duration longer than the relaxation time of the thermocouple. It is an indication, that the beam width is indeed smaller than the dimensions of the tile.

A cooling term can be included in each equation, which is due to the fact, that the tile is mounted on a cooling channel, see figure 6, CAD drawing on the left: the vertically elongated, blue structure is in fact a tube with cooling water. The cooling time constant is of the order of several minutes and was measured, using long acquisition times. Within the short pulse analysis of our experiments, it can be neglected.

The system of equations (1-4) can be solved in time, using a Runge-Kutta fourth order scheme, depending on the parameter values. The Runge-Kutta solver is a subroutine to an optimizer [7], which does a least square fit of the model T_M to the measured signal, using as free parameters: the absorbed intensity p_A, most of the material constants (except C_B, A_{SM}, A_{tl}, which can be measured) and the fractions f_{NB} and r_{IB} (f_{IB} is indeed irrelevant due to our choice to ignore the incoming radial transfer from the near bulk).

4 Experimental results

In this paper we restricted the evaluation to a short pulse analysis, assuming the absorbed mm-wave intensity p_A constant during each pulse. It is necessary to calibrate the system in vacuum, measuring the thermocouple response with respect to a well-defined incoming beam power. We neglect the influence of the incoming wave polarisation, because (a) the gratings are optimized to be independent on the polarisation [2] and (b) the reflection geometry and, thus, the angles of incidence are nearly constant. The possible dependency on the polarisation is, therefore, expected to be small.

4.1 Launcher sweep and vacuum calibration

It is possible that the beam will be deflected due to beam refraction in the plasma, and therefore we continuously scan the beam across the thermocouple. For that purpose, we use one of the fast steerable launchers of AUG in segment 5 (cf. figure 2). During one sweep of the launcher mirror, we apply 5 pulses of Gyrotron power, which end up on different positions across the thermocouple (figure 9).

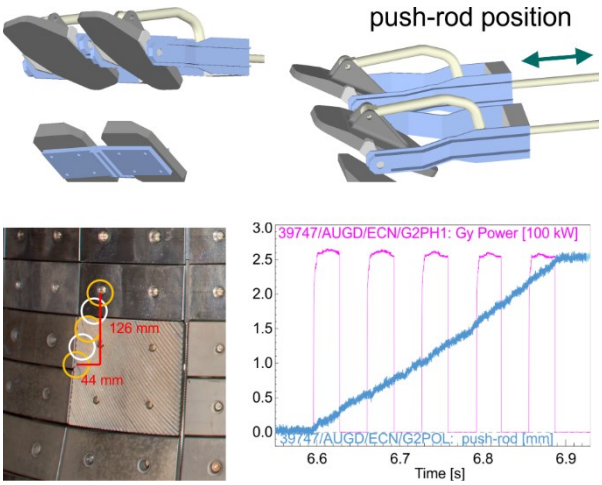

Fig. 9. Exemplary visualisation of the applied mm-wave power and timing of the launcher sweep. The inclination of the launcher mirror is controlled by the push-rod position (top). Five pulses are applied during one sweep of the launcher. The pulses end up on different positions on the heat shield and around one selected thermocouple of the corresponding reflecting grating (photo bottom left). The timing of the push-rod position and of the applied mm-wave power are shown.

This sweep is large enough to clearly identify the maximum response of the thermocouple to the applied mm-wave power, in both cases with and without plasma (e.g. figure 10). According to the TORBEAM simulation [8], the vertical beam refraction is more important than the horizontal one. A fast horizontal sweep is technically not possible with this launcher.

The signal quality in the vacuum case (figure 10) is very good, such that the free parameters (section 3.2) can be fitted together with the pulse amplitudes. The parameter values of the fit result seem reasonably consistent: e.g. C_{SM}/k_{SM} = 30 ms, corresponding to the main time constant of the thermocouple measurement.

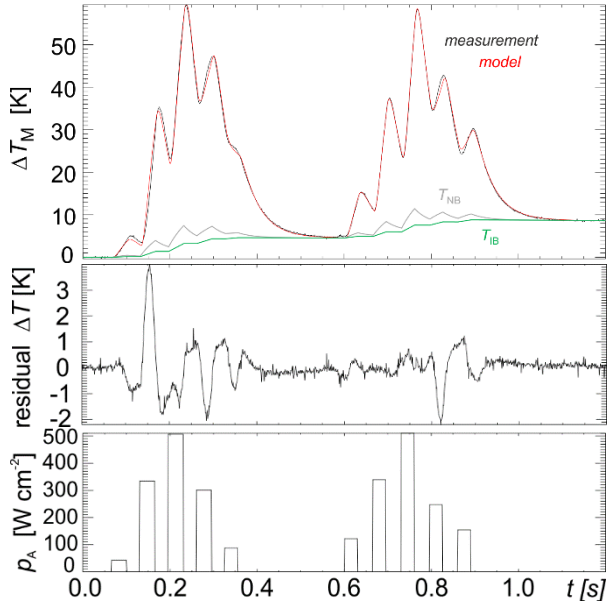

Fig. 10. Measured signal response to pulses of mm-wave power without plasma, compared with the modelling. Pulse amplitudes (bottom row) are the fit results. The main part of the residual (middle row) can be understood from the fact, that the model intensity amplitude is assumed to be constant within one pulse. In reality, during the fast launcher sweep for example in the second pulse (at approx. 0.15 sec) the absorbed mm-wave intensity increases during the measurement. The model fits an average value and, therefore, the residual, which is model minus measurement, is positive during the first part of the pulse. The observer should keep in mind, that there is a time lag between the mm-wave power and the measurement. The data was recorded as AUG experiment #39744.

The fitted quantity k_{SM}/A_{SM}=15000 W/(K m^2) can be approximated by λ/d where λ is the specific heat conductivity and d the distance between the absorbing surface and the measurement position (T_M). In the case of a typical insulator with λ approx. 1 W/(K m) this corresponds to d of the order 10^{-4} m, which is consistent with the specification of the thermocouple [6].

An additional fitted signal delay of the order of 1 ms of the thermocouple measurement with respect to the power improves the fit quality. It should also be mentioned, that the fit of parameters, which are related to material constants, is part of the calibration. When evaluating a measurement, only beam related quantities should be fitted again, i.e. pulse amplitudes p_A and the fraction to the intermediate bulk r_{IB}.

4.2 Absorption measurement X-3

Experiments were carried out to measure the plasma absorption at the X-3 resonance as a function of the plasma electron temperature. We show an exemplary overview of experimental data in figure 11. Heating and X-3 probing geometry are visualized in figure 12. For further evaluation see the contribution by J. Stober [9]. The signal evaluation as described in section 4.1 yields the results of figure 13. The material constants from the vacuum calibration are used. Fit results are: p_A (one value for each pulse) and r_{IB} (only one value for the entire time interval). If the absorbed power during one pulse is not constant, then deviations between model and measurement can be observed in the residual, e.g. during the longer pulse at t approx. 4.9 sec, where the background plasma (cf. figure 11) seems to be transient.

In order to evaluate the X-3 absorption, the fitted p_A with plasma (figure 13) are normalised by the launched Gyrotron power of Gyrotron 6 (figure 11) and the five pulses during one launcher sweep are summed up. The same procedure is done in the vacuum case, where in particular the launched Gyrotron power was different. The shine through is evaluated by the ratio of the plasma measurement versus the vacuum measurement.

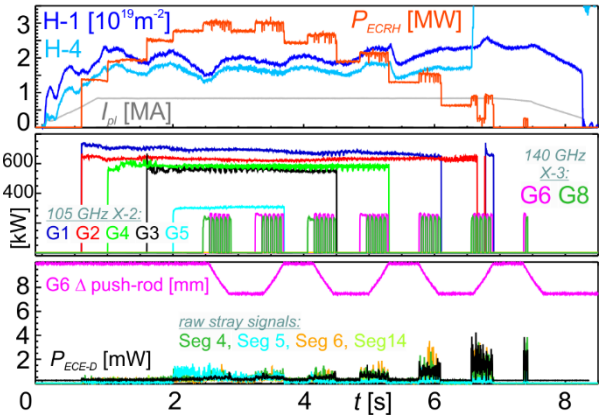

Fig. 11. Comprehensive overview of AUG discharge #39747 with total ECRH power data, evolution of plasma density and plasma current on top, individual Gyrotron power signals in the middle row, and Launcher 6 push-rod scans, as well as stray radiation signals in the bottom row. The blue density signals on top are line-integrated interferometry data. Middle row: the purpose of the group of 105 GHz Gyrotrons is to vary the plasma heating such, that different levels of plasma electron temperature exist. Bottom row: Stray radiation, in particular which is measured by the ECE, is significant only during the 140 GHz X-3 pulses and increases with decreasing plasma electron temperature, as expected.

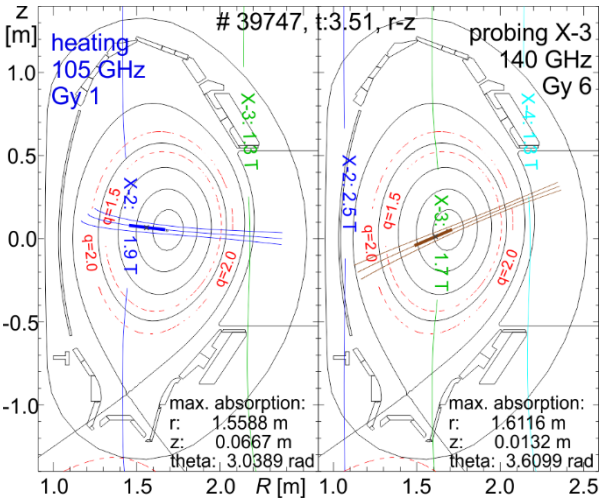

Fig. 12. Cross section, AUG #39747 showing the geometry [8] of the 105 GHz X-2 heating (left) and the 140 GHz probing (right). The main magnetic field strength was chosen such, that for 140 GHz only the X-3 resonance is present in the plasma. The heating beams (left) were launched with a toroidal angle, so that the Doppler shifted resonance is closer to the centre.

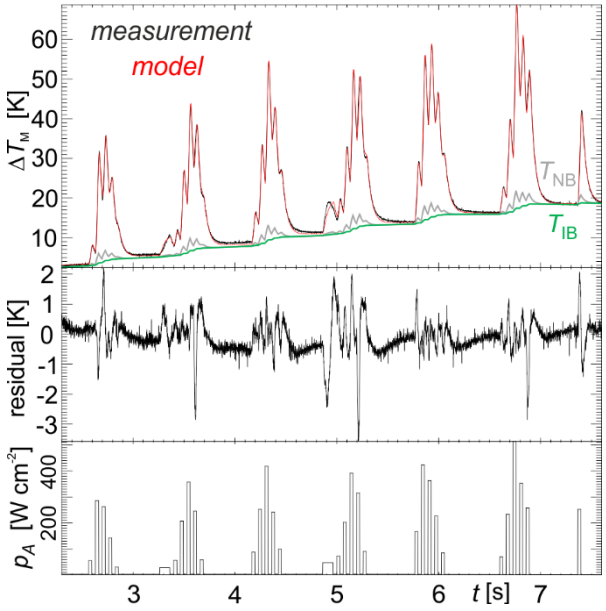

Fig. 13. Evaluation of thermocouple measurement, AUG #39747 showing in the top row: measurement (black) and the temperature at the model grid points T_M (red), T_{NB} (grey), T_{IB} (green). The amplitudes of the model temperature T_{SM} are much larger and not shown for simplicity. Second row: residual = model temperature minus measurement. The residual is subject to minimization in the fit procedure using the p_A as fit parameters. The resulting p_A are shown in the bottom row. The parameter r_{IB} was also fitted, but assumed constant during the experiment.

4.3 Shine-through power in O-2 polarisation

The evaluation model described in section 3.2 was developed very recently. Earlier, the amplitude of the pulse response of one thermocouple to the pulsed mm-wave power in O-Mode was recorded as a function of the launching direction (figure 14).

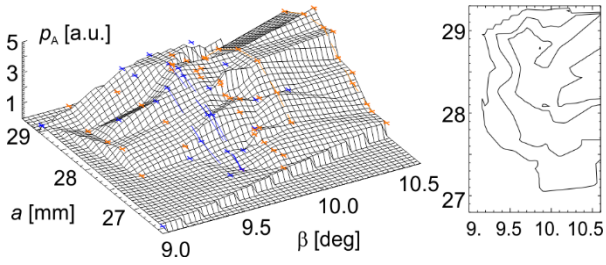

Fig. 14. Pulse amplitude response of one thermocouple on the reflecting grating of Gyrotron #8 to TORBEAM [8] evaluated O-2 mode shine through power as a function of the push-rod position *a* [mm] and the rotation of the mirror support around the push-rod β [deg]. The plot on the left was generated using Delauney triangulation and corresponding visualization [7] for irregularly gridded data. Individual measurements are plotted in orange (2017 campaign) and blue (2019 campaign). Points connected with a dashed line are from a launcher sweep as described in section 4.1. The inset on the right is a contour plot of the same data, with contour levels 0.9, 1.8, 2.7 and 3.6. Within the plot range of *a* [mm], the centre of the beam moves approx. 10 cm on the heat shield, and approx. 7 cm within the plot range of β. The coordinates are only approximatively corresponding to the vertical and horizontal directions, because the geometry is oblique (cf. figure 9).

This was repeated in a particular plasma experiment called "Standard H-mode", which is carried out frequently and considered reproducible. Short pulses (approx. 30 ms) of Gyrotron no. 8 (Elisey 3M) were used for these experiments. Vacuum calibration data were not measured. Figure 14 shows data from the 2017 and 2019 experimental campaigns. With the thermocouple position being fixed, it should be possible to transform the variation of the launching direction into a cross section of the shine-through beam. This needs beam tracing and reliable plasma kinetic profiles in order to evaluate the shine-through power. We propose to use the simplified analysis as shown in figure 14 in order to verify the launcher setting.

5 Summary

The thermocouple mount and the corresponding evaluation model were developed further in order to provide a measuring tool to study mm-wave deposited power on the heat shield of ASDEX Upgrade with high time resolution. A local monitoring of shine-through intensity was demonstrated exemplarily. A systematic comparison of the beam geometry and size with beam tracing predictions seems possible.

Careful mechanical work by H. Schütz is gratefully acknowledged. Photos in figures 6 and 7 as well as the launcher CAD model (figure 9) are also courtesy of H. Schütz. This work has been carried out within the framework of the EUROfusion Consortium, funded by the European Union via the Euratom Research and Training Programme (Grant Agreement No 101052200 — EUROfusion). Views and opinions expressed are however those of the author(s) only and do not necessarily reflect those of the European Union or the European Commission. Neither the European Union nor the European Commission can be held responsible for them.

References

1. P. Lang, *et al.*, Nucl. Fusion **59**, 026003 (2019)
2. H. Höhnle, *et al.*, Nucl. Fusion **51**, 083013 (2011)
3. M. Schubert, *et al.*, EPJ Web Conf **203**, 02009 (2019)
4. W. Kasparek, *et al.*, Int. J. Infrared Millim. Waves **22**, 1695 (2001)
5. M. Schubert, *et al.*, 43rd Conf. Plasma Phys, ECA **40A**, P1.026 (2016)
6. RÖSSEL-Messtechnik GmbH, *Mantelthermo-elemente*, Produktinformation 071 (12/2020)
7. ITT Visual Information Solutions, *IDL Version 7.1 Reference Guide* (2009)
8. E. Poli, A. Peeters, G. Pereverzev, Comput. Phys. Commun. **136**, 90 (2001)
9. J. Stober, et al., *Quantification of X3 absorption for ITER L-mode paramteres in ASDEX Upgrade*, these conference proceedings (2022)